Studying Reduction in Solid Oxide Fuel Cell Activity with Density Functional Theory− Effects of Hydrogen Sulfide Adsorption on Nickel Anode Surface

ARTICLE *in* THE JOURNAL OF PHYSICAL CHEMISTRY C · OCTOBER 2007

Impact Factor: 4.77 · DOI: 10.1021/jp072450k

3 AUTHORS, INCLUDING:

Natasha Galea
University of South Wales
17 PUBLICATIONS **296** CITATIONS
SEE PROFILE

Thomas Ziegler
The University of Calgary
388 PUBLICATIONS **23,284** CITATIONS
SEE PROFILE

Studying Reduction in Solid Oxide Fuel Cell Activity with Density Functional Theory−Effects of Hydrogen Sulfide Adsorption on Nickel Anode Surface

Natasha M. Galea, Eugene S. Kadantsev, and Tom Ziegler*

Department of Chemistry, University of Calgary, University Drive 2500, Calgary, Alberta, T2N 1N4 Canada

Received: March 28, 2007; In Final Form: June 19, 2007

To gain insight into the degree by which sulfur-based contaminants poison the solid oxide fuel cell (SOFC) anode, we examine adsorption and dissociation of consecutive molecules of hydrogen sulfide on a nickel (111) surface. Preferred adsorption sites, energies, transition states, and kinetic barriers are calculated for the resulting species, $*SH_x$ ($x = 0 - 2$) and *H. Systematically larger amounts of adsorbed sulfur (0, 25, 50, 75, 100%) are calculated to determine the most energetically favorable sulfur surface coverage. The removal of existing sulfur surface atoms is studied to probe the irreversibility of the hydrogen sulfide adsorption reaction. The extent of molecular hydrogen adsorption at increasing surface sulfur coverages allows us to conclude that the presence of even 25% surface sulfur can reduce molecular hydrogen adsorption on the surface by half. Concurring with experimental data, our research demonstrates equilibrium coverage of 50% adsorbed sulfur on the surface. Due to the considerable exothermic nature of the hydrogen sulfide adsorption and dissociation reaction, partial irreversibility of the reaction is exhibited. This irreversibility proves challenging during attempts to remove surface sulfur and regain the original electrochemical activity.

1. Introduction

In today's technology, fuel cells represent a viable replacement for existing power sources.[1] Operating with no polluting emissions and in an efficient manner, fuel cells ultimately offer the production of cleaner energy. Mass market commercial production remains a future objective due to cost and stringent operating conditions that must be currently met to maintain optimum fuel cell activity. All fuel cells are electrochemical cells that are basically comprised of three main sections: two electrodes (cathode and anode) surrounding an electrolyte. The distinguishing features between different fuel cells concern the anode fuel required, the operating temperature of the fuel cell, and the means by which the electrolyte carries ions between the electrodes. The solid oxide fuel cell (SOFC) is a high-temperature (800−1000 °C) device that utilizes hydrogen or hydrocarbons as the anode fuel.[1] Air (O_2(g)) is introduced into the cathode, adsorbs, and dissociates on the surface where it is reduced to form O^{2-} ions at the cathode triple-phase-boundary (TPB). At the anode, the fuel is adsorbed and dissociates on the anode surface, along with any impurities in the fuel source. Hydrocarbon fuels, for example, methane, must undergo steam reforming reactions before they can be adsorbed, to allow for their transformation to hydrogen and carbon monoxide.[1] Because of high SOFC operating temperatures, the O^{2-} ions migrate from the cathode TPB, through the electrolyte, to the anode TPB where oxidation occurs. Adsorbed hydrogen and/or hydrocarbons undergo oxidation to produce electrons and water and/or carbon dioxide, respectively. The electrons travel externally from the anode to the cathode and are used to reduce further oxygen species at the cathode TPB. This use of internally generated electrons completes the cycle, overall creating electrochemical activity and electrical power within the cell.

Sulfur-based compounds are known to cause SOFC electrode degradation and, therefore, reduce electrochemical performance.[1] Despite containing high concentration levels of contaminants such as hydrogen sulfide (H_2S(g)), hydrocarbon anode fuels are commonly utilized within a SOFC. It has been reported that H_2S(g) within the anode fuel must be maintained at a concentration <1 ppm to sustain a reasonable SOFC lifetime.[2] However, most commonly available hydrocarbons contain much higher levels of sulfur and require the application of costly, complex desulfurization reactions to overcome sulfur poisoning of the fuel cell. Currently, a nickel composite (nickel−yttria-stabilized-zirconia, Ni−YSZ) is the most commonly used SOFC anode material.[1] Despite several experimental[3−21] and theoretical[21−25] studies concerning adsorbed sulfur species on nickel surfaces, little has been published in terms of theoretical studies on the manner and degree by which sulfur-based contaminants affect the performance of a SOFC.

On any metal surface, there are only a finite number of vacant sites that are available for adsorption. The adsorption of fuel impurities (e.g., H_2S(g)) onto the anode surface reduces the number of adsorption sites available for hydrogen and/or carbon. Adsorption of H_2S(g) poisons the surface, eventually reducing the electrochemical activity of the cell. Even in earlier literature, the blocking of vacant adsorption sites was considered the main mechanism behind sulfur poisoning.[7] On the basis of a number of different experimental reactions, the catalytic activity of a nickel surface is established to decrease due to the adsorption of sulfur.[6,7,16a,19,20] Sasaki et al.[19] have recently published comprehensive experimental data concerning H_2S(g) poisoning of the Ni−YSZ anode. At operating temperatures of 1000 °C, Sasaki demonstrated that overall electrochemical cell activity (voltage) decreased by continuously larger amounts corresponding to increased H_2S(g) concentration (up to 5 ppm) in the anode feed. Saturation occurred at a concentration of 5 ppm, and no additional reduction in activity was observed upon increasing

* To whom correspondence should be addressed. E-mail: ziegler@ucalgary.ca.

10.1021/jp072450k CCC: $37.00
Published on Web 09/08/2007

the $H_2S(g)$ concentration in the anode feed further. This experimental data is further supported by studies by the Birss experimental group.[20] Both groups have illustrated that temperature plays an important role in sulfur poisoning of the nickel surface. At temperatures greater than 850 °C, Sasaki found that cell activity decreased but became stable within a few minutes.[19] Below 850 °C, the decrease in cell activity did not stabilize and was accompanied by irreversible poisoning (decrease in cell voltage could not be recovered by removing the hydrogen sulfide impurities from the anode fuel feed). Birss considered thermogravimetric analyzer (TGA) analysis on Ni−YSZ samples with a H_2/He fuel ratio set to 20:80 and a $H_2S(g)$ concentration of 5 ppm.[20] Comparing temperatures in the range of 500−900 °C, the extent of sulfur poisoning on nickel decreased with increasing temperature. While several research groups have demonstrated that sulfur adsorption on a nickel surface is a reversible process,[7,16a,19,20] some believe that complete removal of adsorbed sulfur from the surface cannot be attained.[16a,19,20] This reaction irreversibility creates problems when attempting to remove previously adsorbed sulfur from the surface to regain the original electrochemical activity. If even partial irreversible poisoning of the surface occurs, the strongly adsorbed sulfur must be removed from the surface using other methods to achieve the original activity, such as desorption of elemental sulfur[15] and oxidation.[9] While most research groups have determined that the maximum sulfur surface coverage that can be achieved is around 50−60%,[4,5,7−11a,16a] further adsorption has led to the formation of a physisorbed layer of H_2S above the surface.[10,11a] The percentage sulfur surface coverage is the number of adsorbed sulfur atoms divided by the number of surface nickel atoms, times 100. Recently published theoretical research by Choi et al.[23a] and Albenze and Shamsi[25] considered hydrogen sulfide adsorption and dissociation on a nickel planar surface (eqs 1−4). Through the use of periodic calculations, the Choi group[23a] determined that the production of a sulfur surface coverage of 25% released ∼50 kcal/mol via a dissociative (compared to molecular) adsorption mechanism. Albenze and Shamsi,[25] also using periodic calculations, considered only a molecular adsorption mechanism to produce an initial sulfur surface coverage of 11%. The molecular adsorption reaction studied by Albenze and Shamsi established an almost identical energy pathway to that produced by Choi. This demonstrates the ease with which hydrogen sulfide adsorbs on a planar nickel surface and the exothermic nature of the driving force behind the reactions that produce adsorbed sulfur (*S) and hydrogen (*H) on the surface. This data is backed up experimentally by several groups who demonstrated that hydrogen sulfide adsorption, up to a sulfur surface coverage of 50%, is followed by complete dissociation of the adsorbed species, producing *S and *H.[4,11a] At low sulfur surface coverages, the $*SH_2$ and *SH adsorbed species quickly dissociate (eqs 3 and 4). Ease of dissociation results in their lack of appearance during experimental reactions studying the adsorption and dissociation of hydrogen sulfide.[11a] The corresponding reaction at sulfur surface coverages greater than 50% allows the observation of $*SH_2$ and *SH due to greater species stabilization produced by larger dissociation barriers.[4,11a]

$$H_2S(g) + \text{Surface} \leftrightarrow *SH-*H \quad (1)$$

$$H_2S(g) + \text{Surface} \leftrightarrow *SH_2 \quad (2)$$

$$*SH_2 \leftrightarrow *SH-*H \quad (3)$$

$$*SH-*H \leftrightarrow *S-*H-*H \quad (4)$$

The objective of the research reported here has been to consider the adsorption of consecutive molecules of hydrogen sulfide gas onto a planar nickel (111) surface, producing sulfur surface coverages of up to 75%. The most energetically feasible sulfur surface coverage on a nickel surface is studied to determine the optimum coverage. The irreversibility of hydrogen sulfide surface adsorption is examined to establish whether it is possible to regain the original electrochemical activity lost during anode poisoning. The study of desorption reactions of molecular hydrogen, at different sulfur coverages, finally attempts to determine the degree of reduction in possible cell activity that occurs when sulfur is adsorbed on the surface.

2. Method

2.1. Methodology for Density Functional Theory (DFT) Calculations. Kohn−Sham DFT calculations were performed using the Vienna Ab initio Software Package[26] with plane-wave basis set and an orthorhombic supercell geometry. Each slab consisted of three layers of atoms with the (111) surface represented by a 2×2 unit cell. The slabs were separated in the direction perpendicular to the surface by a vacuum region of ∼10 Å. The ion−electron interaction was treated using the projector augmented wave[27] (PAW) method. All calculations were spin-polarized. The exchange-correlation effects were treated within the generalized gradient approximation with PBE96[28] exchange correlation functional. The brillouin zone was sampled using $5 \times 5 \times 1$ Monkhorst−Pack[29] mesh. The (wave function) kinetic energy cutoff was set to 400 eV and the (augmentation) charge density cutoff was set to 800 eV. For geometry optimization searches within each reaction step, all metal atoms were fixed in the slab geometries at their bulk-truncated positions in a face-centered cubic (fcc) lattice with a theoretical equilibrium bulk lattice constant of $a_O = 3.52$ Å. It should be noted that the theoretically calculated and the experimentally determined bulk lattice constant (a_O) are nearly identical.[30] Once the optimum geometry was determined for each reaction step, coordinates were reoptimized while relaxing the top nickel surface layer to calculate more accurate minima energy. Geometries were optimized until the energy had converged to 10^{-3} eV. All transition states and reaction barriers were calculated with the nudged-elastic band[31] method.

2.2. Methodology for Determining Rate of Reactions. Rate of reaction calculations were performed using the mathematical software program MatLab.[32] An overall reaction process is modeled by describing each individual reaction step using its corresponding kinetic barrier (ΔH). The rate constant, k, for each forward and backward reaction is calculated based on the Eyring equation

$$k = \frac{k_B T}{h} \exp\left(-\frac{\Delta G}{RT}\right) \quad (5)$$

and the Gibbs' free energy, ΔG, of the corresponding kinetic barrier

$$\Delta G = \Delta H - T\Delta S \quad (6)$$

Here k_B is the Boltzmann constant, h is Planck's constant, R is the universal gas constant, T is temperature, ΔH is enthalpy, and ΔS is entropy. When calculating rate constants for barrierless reactions, a zero-energy barrier is assumed, basing the rate constant on the approximate pre-exponential factor.

Entropy (ΔS) is a temperature-dependent energy contribution based on the movements of atoms and bonds in a compound. While entropy is comprised of translational, rotational, and vibrational components, the percentage contribution of each component is not equal. In the gas phase, translation and rotation contribute the greatest amount of energy toward the overall entropy of a molecule. When a gas-phase molecule is adsorbed on a surface, the movements of the respective atoms and bonds are restricted, substantially decreasing the energy contribution from translational and rotational energy. Calculating the entropy of adsorbed species using periodic DFT calculations and PAW potentials is not currently viable. One method to approximate the entropy of an adsorbed species is to assume that all translational and rotational energy of the gas molecule is lost/gained upon adsorption/desorption. In turn, this assumes that the vibrational energy of the gas molecule is preserved during adsorption/desorption and is carried through during subsequent surface reactions. In practice, this method determines that the difference in entropy between a gas-phase molecule and the respective adsorbed species is equal to the translational and rotational energy found in the gas-phase molecule. Vibrational energy is considered to "cancel out", as it is assumed to exist in identical amounts in all gas phase and surface-adsorbed compounds. When calculating the Gibbs' free energy (ΔG, eq 6) of a surface or adsorbed species, ΔS equals zero and therefore ΔG equals ΔH. The entropy contribution of gas-phase molecules (molecular hydrogen and hydrogen sulfide) differs depending on the molecule in question. Geometry and frequency calculations were carried out to determine gas-phase entropy using the Amsterdam density functional (ADF 2004) program developed by Baerends et al.[33] and the Becke−Perdew[34] exchange-correlation functional. Calculated entropy (translational and rotational energy) data are $\Delta S_{\text{Transl+Rot}}(H_2(g)) = 0.03118$ kcal/mol/K and $\Delta S_{\text{Transl+Rot}}(H_2S(g)) = 0.04913$ kcal/mol/K.

Sun et al.[35] have calculated the difference in entropy between $H_2S(g)$ and $H_2(g)$ and the respective adsorbed species on NiMoS edge surfaces using DFT calculations utilizing effective core potentials. During adsorption of molecular hydrogen, a 75% loss in overall entropy was calculated. Adsorption of the larger gas molecule hydrogen sulfide produced a 70% loss in entropy. One main assumption in our method is the premise of 100% loss/gain in translational and rotational energy during the formation of an adsorbed species. While this assumption may not be completely accurate, it does allow the determination of the maximum possible change in entropy that can occur during adsorption/desorption reactions.

The individual rate constants are used to determine the time-dependent rate of formation of each individual species in the reaction scheme. Concentration of each individual species is calculated by integrating the respective rate of formation over time t. In this fashion, at time t the concentration of each species is determined based on the respective concentration of all other species. MatLab is a mathematical suite of programs that allow multiple equation rate of formation calculations to be simultaneously integrated.[32]

3. Results and Discussion

3.1. Testing: Hydrogen Sulfide Adsorption Producing 25% Surface Coverage of Adsorbed Sulfur. As an initial step of our investigation, we duplicated the previously published calculations concerning the adsorption of one molecule of hydrogen sulfide gas on a planar nickel surface.[23a,25] This allowed us to compare results from different approaches (different software packages, functionals, supercell size, etc.).

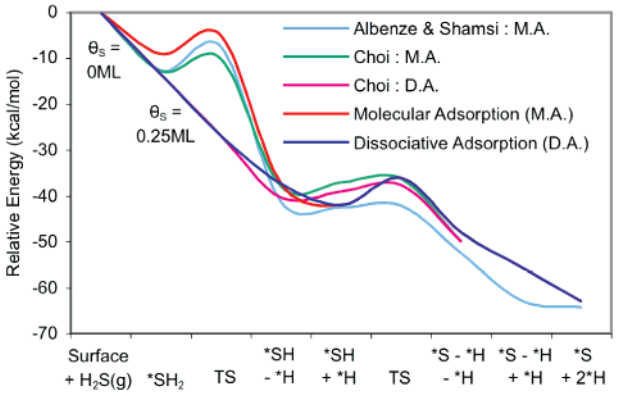

Figure 1. Thermodynamic and kinetic data for molecular and dissociative adsorption and dissociation of $H_2S(g)$ on a nickel (111) planar surface; a comparison of research with published work by Choi et al.[23a] and Albenze and Shamsi.[25]

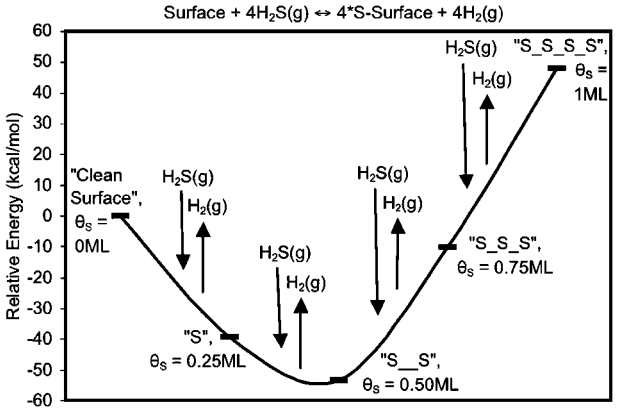

Figure 2. Thermodynamic energy profile for consecutive adsorption/desorption of $H_2S(g)/H_2(g)$ on nickel (111) surface, resulting in differing amounts of adsorbed sulfur surface coverage ($\theta_S = 0-1$ ML).

The comparative data (Figure 1) demonstrates good energy agreement between the different research groups, while any discrepancies in the data are small and within calculation error. On the x-axis of the graph (Figure 1), a label in the form "*A − *B" illustrates steric interaction between the adsorbed species "*A" and "*B". The corresponding label "*A + *B" demonstrates no surface steric interaction between the respective species.

3.2. Maximum Adsorbed Sulfur Surface Coverage (θ_S). Due to the importance of the large steric interactions between the neighboring atoms adsorbed on the surface, the largest, most thermodynamically feasible surface sulfur coverage percentage was determined. The most energetically favorable positions for sulfur adsorption on a planar nickel (111) surface are fcc three-fold-hollow (3fh) or hexagonal close-packed (hcp) three-fold-filled (3ff) sites.[22−25] In theory, there are two three-fold (3f) adsorption sites for every one nickel atom on the Ni(111) surface. In reality, due to the large size of the sulfur atoms and therefore large steric interactions between neighboring atoms, there is only one 3f site available for sulfur adsorption for every one nickel atom on the planar surface. Purely on the basis of thermodynamic data (Figure 2), the most stable sulfur coverage on a planar nickel (111) surface is $\theta_S = 0.50$ ML (50%). Adsorbed sulfur surface coverage (θ_S) is the ratio between the number of adsorbed sulfur atoms and the number of surface nickel atoms. A surface coverage of 100% is represented as nS/nNi = 1.00 ML (n = number of sulfur or nickel atoms).

The theoretically determined percentage of adsorbed sulfur on the surface concurs with previously recorded experimental

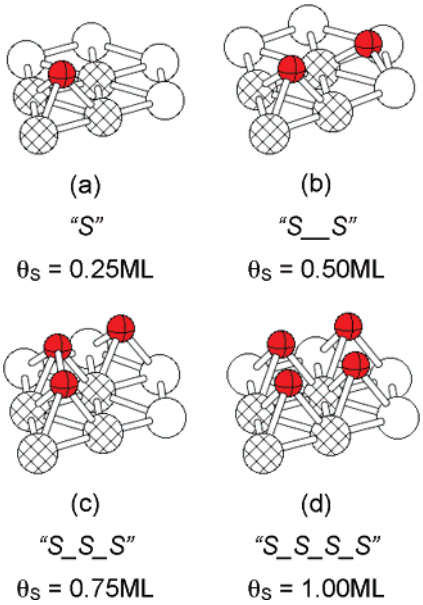

Figure 3. Simplified geometries illustrating different amounts of adsorbed sulfur (θ_S) on nickel planar surface layer. 2 × 2 supercell highlighted by patterned nickel nuclei.

literature, demonstrating maximum adsorption on a nickel surface to be between 0.50 and 0.60 ML.[4,5,7−11a,16a] This demonstrates that the planar nickel surface has a natural cutoff point that controls the maximum sulfur coverage that can be adsorbed on the surface. Further adsorption of sulfur on the surface, after this maximum surface coverage has been attained, requires the input of a substantial amount of energy and is thus not feasible. Sasaki et al.[19] and the Birss research group[20] have studied the effects of small amounts of hydrogen sulfide in the anode fuel (i.e., H_2(g) ∼1 atm/H_2S(g) ∼1 × 10^{-5} atm (10 ppm)). The presence of hydrogen sulfide gas causes a decrease in activity but not a complete shutdown of the cell. The thermodynamically determined natural cutoff point controlling the amount of adsorbed sulfur on the surface can explain this. Sulfur adsorbs on and therefore blocks 50% of the nickel surface, but this still leaves a remaining 50% of adsorption sites available for further adsorption of a small molecule such as molecular hydrogen.

The geometries of the energetically most favorable structures within the different surface sulfur coverage's (θ_S) are illustrated in Figure 3. A coverage of 0.25 ML (Figure 3a, "S") reveals a sulfur atom adsorbed at a 3fh position on the planar nickel surface. The corresponding Ni−S (×3) bond distances are 2.15 Å, and this is coupled with S−S distances greater than 4 Å. At this particular surface coverage, using a 2 × 2 supercell, the adsorbed sulfur atoms are too far apart on the surface to exert influence on each other. The relaxed nickel surface has Ni−Ni bond distances between 2.44 and 2.54 Å. This demonstrates elongation and constriction of the bonds when compared with the frozen nickel bond distances in the bulk or the relaxed clean (θ_S = 0 ML) surface (Ni−Ni bond distances are 2.49 Å in both cases). Around the adsorbed sulfur atom, the Ni−Ni bond distances are 2.54 Å, illustrating a weakening of the surface Ni−Ni bonds upon adsorption of sulfur. Despite relaxation of the top surface layer, the corresponding nickel atoms are completely planar.

Adsorption of two sulfur atoms (Figure 3b, "S−−S") at opposite 3fh and 3ff sites on the supercell, θ_S = 0.50 ML surface, displays relaxed Ni−Ni bond distances between 2.46 and 2.54 Å. Adsorption at these symmetrical sites on the surface allows the least steric interaction between the sulfur atoms. S−S distances within the "S−−S" structure are a minimum of 3.12 Å. The S−S distance is substantial enough to cause interactions between the sulfur atoms on the surface. This is demonstrated by thermodynamic data (Figure 2); production of a θ_S = 0.25 ML surface releases 39 kcal/mol of energy, but formation of a θ_S = 0.50 ML surface releases only an additional 14 kcal/mol of energy. Both sulfur atoms are surrounded by a triangle of nickel atoms with Ni−Ni bond distances of 2.54 and (×2) 2.50 Å (S_{3ff} produces (×2) 2.48 Å). Corresponding Ni−S bond distances are 2.10 and (×2) 2.13 Å. These data imply that the stronger the sulfur absorption on the surface, the weaker the surface bonding of the surrounding nickel atoms. The "S−−S" species also illustrates an increase and decrease in the height of the nickel atoms in the relaxed surface layer, when compared to a frozen bulk layer. This phenomenon, also observed further on in the *S−*SH−*H species, occurs due to the adsorption of sulfur atoms at 3fh and 3ff sites on opposite sides of a central surface nickel atom. Because of strongly adsorbing sulfur centers, nickel nuclei bonded to two adsorbed sulfur centers are raised above the surface by ∼0.16 Å. Nickel nuclei that are bonded to only one adsorbed sulfur center are lowered by ∼0.07 Å. Overall this creates a relaxed zigzag nickel surface layer where the sulfur atoms are all at an equal height to each other due to the differing Ni−S bond distances described above. This "lifting" of first layer surface atoms, due to sulfur surface adsorption, has been observed experimentally on a Ni(100) surface by Oed et al.[12]

Both the θ_S = 0.75 ML and θ_S = 1.00 ML surfaces have been previously illustrated to be energetically unfavorable (Figure 2). While all three atoms on the θ_S = 0.75 ML surface (Figure 3c, "S_S_S") are approximately adsorbed in 3fh positions, two sulfur atoms are positioned in close proximity to each other with a bond distance (S1−S2) of 2.15 Å. The remaining adsorbed atom (S3) is ∼2.58 Å from the nearest adjacent sulfur atom. The corresponding Ni−S bond distances are as follows: Ni−S3 (×3), ∼2.17 Å; Ni−S1 and Ni−S2 (nickel adsorbed to unbonded S1 and S2) 2.37 Å; and all other Ni−S1 or Ni−S2 bonds ∼2.22 Å. The relaxed nickel surface, while remaining planar, alters its Ni−Ni bond distances to between 2.45 to 2.54 Å. The largest sulfur surface coverage geometrically possible, θ_S = 1 ML, contains sulfur atoms adsorbed at all 3fh sites (Figure 3d, "S_S_S_S"). This species produces a uniform sulfur coverage corresponding to all Ni−Ni and S−S bond distances of 2.49 Å and Ni−S bond distances of 2.27 Å. Geometry within "S_S_S_S" is very similar to bulk nickel with the exception of Ni−Ni bond distances between frozen and surface nickel layers of 2.52 Å, compared to 2.49 Å for the bulk.

3.3. Hydrogen Sulfide Adsorption on a Planar Nickel Surface. The adsorption process studied by Choi et al.[23a] and Albenze and Shamsi[25] (Figure 1) is only the first step (reaching a maximum sulfur surface coverage of θ_S = 0.25 ML) in the overall adsorption and dissociation of hydrogen sulfide gas on a nickel planar surface. Many gas molecules of hydrogen sulfide adsorb on nickel, eventually covering 50% of the surface and causing the decrease in electrochemical activity that is noted experimentally. Therefore, our second objective was to follow the thermodynamic and kinetic path to produce a sulfur surface coverage of θ_S = 0.50 ML via the adsorption of a second hydrogen sulfide molecule. Hydrogen sulfide adsorption, producing a θ_S = 0.50 ML surface, creates a very different reaction energy pathway (Figure 4) to that illustrated for a lesser coverage. While the production of the θ_S = 0.25 ML surface is

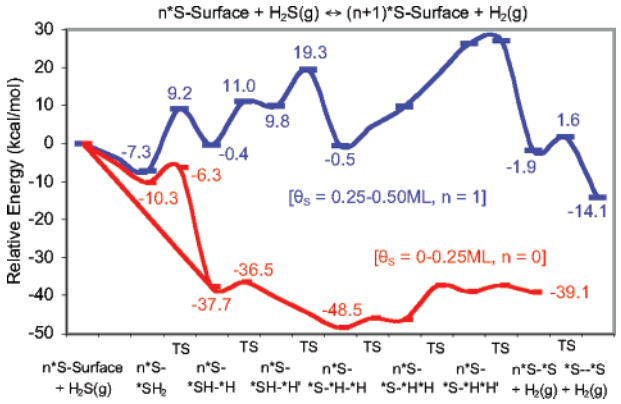

Figure 4. Energy pathway comparing adsorption and dissociation of consecutive molecules of $H_2S(g)$ on a Ni (111) surface, producing a sulfur coverage of $\theta_S = 0.25$ ML ($n = 0$) and $\theta_S = 0.50$ ML ($n = 1$), respectively.

a strongly exothermic reaction (−48 kcal/mol), the formation of a $\theta_S = 0.50$ ML surface is more endothermic in nature with larger associated energy barriers. The presence of adsorbed sulfur has been shown experimentally to increase the corresponding kinetic barriers of reactions on nickel surfaces.[9] Unlike a surface with 0.25 ML sulfur coverage, no dissociative adsorption mechanism was determined for the $\theta_S = 0.50$ ML surface. The most stable species on a sulfur surface of 0.50 ML is produced after the desorption of molecular hydrogen (2*S species). This differs completely from the $\theta_S = 0.25$ ML surface in which the most thermodynamically stable species contains individually adsorbed S and H atoms (i.e., *S−*H−*H). Comparing the corresponding hydrogen sulfide adsorption and molecular hydrogen desorption reactions on both surfaces, a 0.25 ML sulfur surface favors the presence of hydrogen on the surface, but a $\theta_S = 0.50$ ML surface will aid the removal of adsorbed hydrogen.

The geometries for the $\theta_S = 0.25$ ML surface (Figure 5a−f) determined by this group are very similar to those of Albenze and Shamsi[25] and are almost identical to those published by the research group of Choi et al.[23a] To produce a 0.25 ML of surface sulfur, hydrogen sulfide adsorbs on the surface via dissociative (eq 1) or molecular (eq 2) adsorption. Dissociative adsorption occurs when the hydrogen sulfide molecule approaches perpendicular to the surface, Figure 5a. Molecular adsorption occurs when a molecule of hydrogen sulfide approaches the surface with the H−S−H plane of the molecule parallel to the surface. The resulting species (*SH_2, Figure 5b) remains in a position parallel to the surface at a one-fold (1f) adsorption site with the two H atoms placed over adjacent distorted 3fh and 3ff geometries. The surface−S distance is 2.18 Å and the (×2) S−H bond distances are 1.36 Å. The first dissociated species *SH−*H (Figure 5d) occurs via the transition state (TS) illustrated in Figure 5c. While the corresponding *SH group lies in a $3fh_S-1f_H$ position, the dissociated hydrogen has migrated to a 3ff site. Ni−SH bond distances are 2.29 and (×2) 2.18 Å, S−H_{SH} bond distance is 1.45 Å, surface−H_{SH} bond distance is 1.75 Å, and Ni−H bond distances are ∼1.67 Å. The S−H_{SH} bond is a little elongated in comparison with the corresponding bond distance supplied by Choi[23a] (1.41 Å). The second hydrogen dissociation reaction occurs (TS, Figure 5e) producing the species *S−*H−*H, Figure 5f. Ni−S bond distances are ∼2.15 Å and Ni−H bond distances are between 1.63 and 1.71 Å. Geometries produced during desorption of molecular hydrogen are discussed further on in this account. The resulting structure, "S", Figure 5g, has been previously described in Section 3.2.

Figure 5h−q illustrates the geometries determined during the production of a $\theta_S = 0.50$ ML surface via the molecular adsorption of hydrogen sulfide. The *S−*SH_2 species (Figure 5h) is very similar to the corresponding structure on the $\theta_S = 0.25$ ML surface (Figure 5b). The *SH_2 group is adsorbed at a 1f site but, in Figure 5h, with the hydrogens in distorted two-fold (2f) positions. The H−S−H plane is parallel to the surface at a more elongated distance of 2.30 Å, compared to 2.18 Å for Figure 5b. Corresponding S−H bond distances are almost identical at (×2) 1.37 Å. The *S group remains in a 3fh position with Ni−S bond distances of 2.19 and (×2) 2.16 Å. Adsorption of a second molecule of hydrogen sulfide, producing a $\theta_S = 0.50$ ML surface, elongates the Ni−S bond distances of the existing sulfur atom. Dissociation of the first S−H bond (TS, Figure 5i) results in the species *S−*SH−*H (Figure 5j) via the migration of the dissociated hydrogen to a 3fh site and the *SH species to a distorted $2f_S-3fh_H$ position. The resulting *SH group is more tightly bound to the surface with Ni−SH bond distances of ∼2.24 Å. The remaining S−H bond retains the same bond length of 1.37 Å as in Figure 5h. The lone hydrogen is bound to nickel atoms on the surface with bond distances between 1.58 and 1.68 Å. The sulfur atoms retain identical nearest S−S distances of 3.16 Å as found in the previous *S−*SH_2 structure. Comparing *S−*SH−*H to the previous structure in the mechanism, the lone sulfur atom is now more strongly bound to the surface with Ni−S bond distances between 2.13 and 2.15 Å. Comparing the n*S−*SH−*H species on both $\theta_S = 0.25$ ML ($n = 0$, Figure 5d) and 0.50 ML ($n = 1$, Figure 5j) surfaces, both S−H and Ni−H have shorter bond distances at greater sulfur coverage implying stronger bonds. Further migration of the hydrogen atom over an adjacent 3ff site to a 2f position (TS, Figure 5k) produces a similar species *S−*SH−*H′ (Figure 5l). In comparison, this species has elongated Ni−SH bond distances, ∼2.26 Å, and Ni−S bond distances between 2.17 and 2.20 Å. The lone hydrogen (2f position) has Ni−H bonds of 1.64 and 1.69 Å. The last S−H bond dissociation reaction in this series (TS, Figure 5m) allows the migration of dissociated sulfur from a 2f position over the bordering 3ff site to an adjacent 3fh position. This dissociation and migration process produces the species *S−*S−*H−*H (Figure 5n), where all the individually adsorbed atoms are in 3fh sites. The resulting symmetrical geometry produces bond distances of Ni−S (×2) 2.22, 2.19 Å and Ni−H (×2) 1.65, 1.61 Å. Both atoms of adsorbed sulfur are more strongly bound to the surface, compared to the single adsorbed sulfur atom on the corresponding species (Figure 5f) of the $\theta_S = 0.25$ ML surface. The geometries produced during desorption of molecular hydrogen are discussed further on in this account. The resulting structure, *S−*S, Figure 5o, is the first of the 2*S species to be produced after the desorption of molecular hydrogen. In comparison to the "S" species previously described in Section 3.2., "S_S" contains more strongly adsorbed sulfur atoms, deduced from Ni−S bond distances, in adjacent 3fh sites. The corresponding bond distances are 2.15 Å (1S adsorbed on Ni atom) and (×2) 2.21 Å (2S adsorbed on Ni atom). The "S_S" structure is not the most stable 2*S species, and so a surface migration process (TS, Figure 5p) involving sulfur occurs to produce "S‗‗S" (Figure 5q). This final structure has been previously described in Section 3.2.

Comparing the adsorption energies of the individual species produced during the consecutive adsorption of two hydrogen sulfide molecules (Table 1) illustrates a reason for the exothermic/endothermic differences observed between the reactions at different sulfur coverages. All the adsorbed species are more

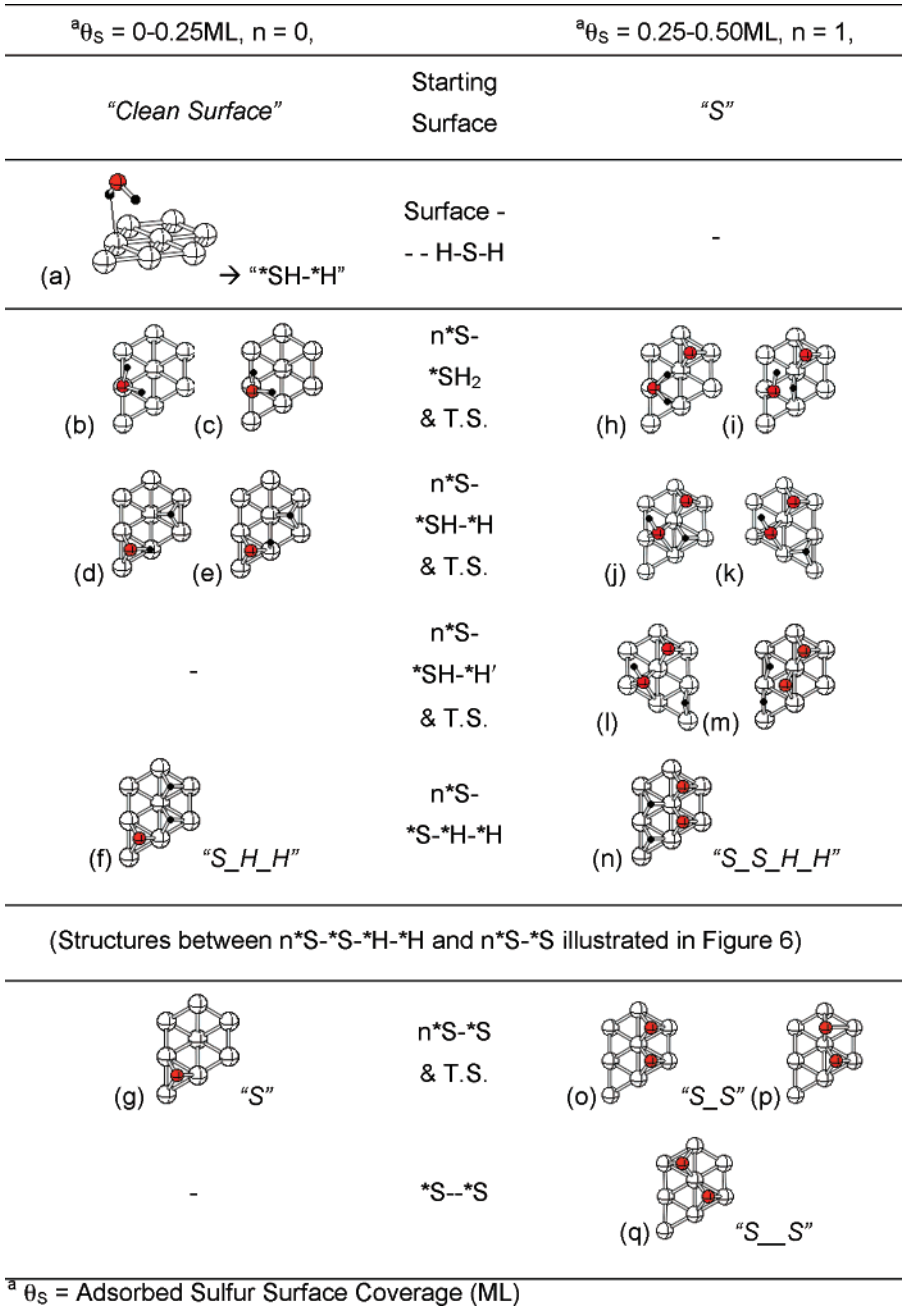

Figure 5. Pictorial representation of geometries upon adsorption and dissociation of H_2S(g) onto a *n**S-surface ($n = 0, 1$).

strongly bound to a $\theta_S = 0.25$ ML surface, compared to larger sulfur surface coverage. This demonstrates that the presence of greater numbers of adsorbed sulfur atoms on the surface weakens the adsorbate bonds, leading to a less stable reaction energy pathway. The adsorption energy of a third molecule of hydrogen sulfide gas adsorbed on the surface (*SH_2, $\theta_S = 0.75$ ML) was also calculated. This demonstrated that not only is a $\theta_S = 0.75$ ML surface thermodynamically unfavorable, but the adsorption energy of the resulting species is so low (negative adsorption energy) that adsorption would not occur. With disregard to the extent of sulfur surface coverage (θ_S), the trend in adsorption energy is as follows: E_{Ads}(*SH_2) < E_{Ads}(*H), E_{Ads}-(*SH) < E_{Ads}(*S).

3.4. Hydrogen Adsorption on Planar Nickel Surface with Differing Surface Sulfur Coverage. The principles behind a hydrogen-based electrochemical cell suggest that the more

TABLE 1: Adsorption Energy of Species *SH_x ($x = 0, 1, 2$) and *H at Differing Amounts of Sulfur Surface Coverage (θ_S)[a]

adsorbed species	Ni(111)−*S−Surface, θ_S before adsorption[a]	adsorption energy, E_{Ads} (kcal/mol)[b]
*SH_2	$\theta_S = 0.00$ ML	10.25
*SH		77.12
*S		115.51
*H		64.17
*SH_2	$\theta_S = 0.25$ ML	7.30
*SH		52.62
*S		90.48
*H		61.00
*SH_2	$\theta_S = 0.50$ ML	−63.89

[a] θ_S = Adsorbed sulfur surface coverage (ML), the ratio between the number of adsorbed sulfur atoms and the number of surface nickel atoms, that is, 2S/4Ni = 0.50 ML = 50% sulfur coverage. [b] $E_{Ads} = E_{Surface} + E_{Gas} - E_{AdsorbedSpecies}$.

[[a]θ_{2H} = 0-0.25ML]	[b]θ_S = 0ML, n = 0,	[b]θ_S=0.25ML,	[b]θ_S=0.50ML,
Starting Surface :	*"Clean Surface"*	n = 1, [c]*"S"*	n = 2, [c]*"S_S"*
TS	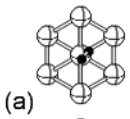 (a)	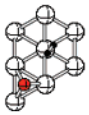 (g)	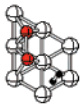 (m)
n*S-*H*H' (HH_1f)	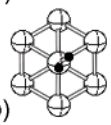 (b)	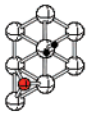 (h)	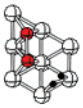 (n)
TS	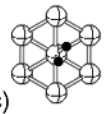 (c)	 (i)	-
n*S-*H*H (HH_3f)	-	 (j)	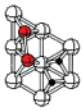 (o)
TS	-	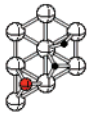 (k)	-
n*S-*H-*H	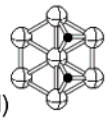 (d) *"H_H"*	(l) [c]*"S_H_H"*	(p) [c]*"S_S_H_H"*
TS	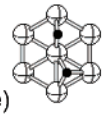 (e)	-	-
*H--*H	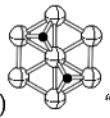 (f) *"H__H"*	-	-

[a] θ_{2H} = Adsorbed Hydrogen Surface Coverage (ML)

[b] θ_S = Adsorbed Sulfur Surface Coverage (ML)

[c] Structures in Figure 5

Figure 6. Pictorial representation of geometries upon adsorption and dissociation of H_2(g) onto a *n**S-surface (n = 0, 1, 2).

hydrogen molecules that adsorb on an anode surface, the greater the number of adsorbed hydrogen atoms available for the oxidation process. In turn, the greater the number of hydrogen atoms oxidized on the surface and the more electrons that are produced, the greater the activity of the electrochemical cell. Sulfur poisoning of the anode surface creates an environment where a decreased amount of hydrogen atoms can adsorb on the surface, ultimately decreasing the overall cell activity. Bartholomew and Pannel experimentally deduced a linear relationship between the amount of sulfur adsorption on a nickel surface and the reduction in the corresponding molecular hydrogen adsorption.[6] This study concluded that no further adsorption of molecular hydrogen occurred once a sulfur surface coverage of 70% was obtained. The third aim of our study considers the geometrical, thermodynamical, and kinetic effects of sulfur coverage (θ_S) on consecutive hydrogen molecule adsorptions. As in the case of sulfur adsorption, hydrogen preferentially adsorbs in 3f sites on the nickel (111) surface. Because of the small size of hydrogen in comparison to sulfur, two hydrogen atoms can adsorb for every one available nickel atom on the planar surface. The adsorbed hydrogen surface coverage (θ_{2H}) is the ratio between the number of adsorbed hydrogen atom pairs (hydrogen atoms studied in pairs in relation to the hydrogen molecule) and the number of surface nickel atoms. A hydrogen surface coverage of 100% represents a n2H/nNi = 1.00 ML hydrogen surface (n = number of nickel atoms or pairs of adsorbed hydrogen atoms).

On a clean surface (Figure 7 and Figure 8), the adsorption of molecular hydrogen is exothermic up to a hydrogen coverage of 50% (θ_{2H} = 2(×2)/4 = 0.50 ML; unit cell adsorption of $2H_2$(g)). Further adsorptions of molecular hydrogen are thermodynamically unfavorable. Adsorption of the first molecule of molecular hydrogen releases 25 kcal/mol of thermodynamic energy and requires 4 kcal/mol of energy to overcome the combined kinetic barriers. The second consecutive adsorption of molecular hydrogen releases an almost identical amount of thermodynamic energy, 23 kcal/mol, while requiring a slightly larger input of energy (7 kcal/mol) to overcome the correspond-

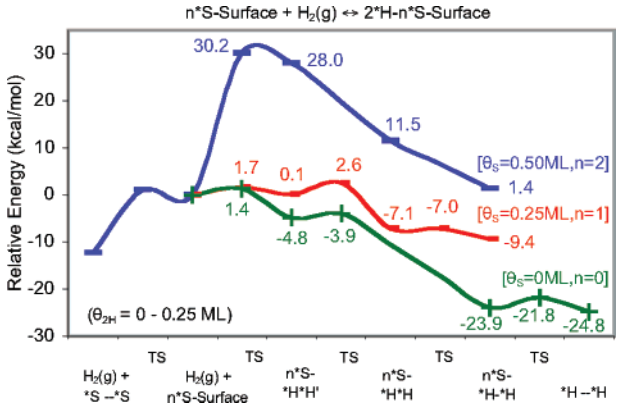

Figure 7. Energy comparison of $H_2(g)$ adsorption ($\theta_{2H} = 0-0.25$ ML) on Ni(111) surfaces with different sulfur surface coverage.

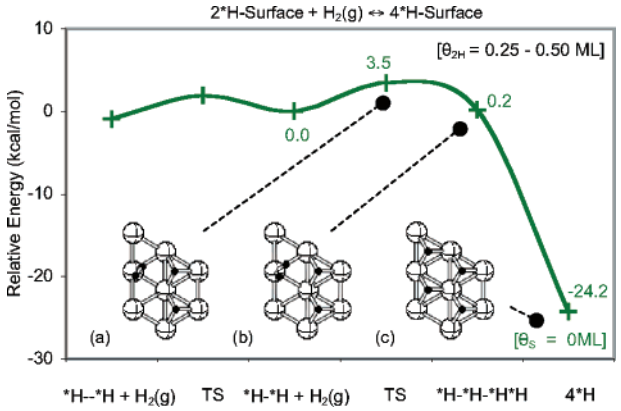

Figure 8. Energies and geometries concerning $H_2(g)$ adsorption ($\theta_{2H} = 0.25-0.50$ ML) on Ni(111) surface.

ing barriers. Therefore, to reach the most energetically stable hydrogen surface coverage without the presence of any adsorbed sulfur requires an energy input of 11 kcal/mol but releases thermodynamic energy amounting to 48 kcal/mol. On a clean surface, production of the most stable hydrogen surface coverage ($\theta_{2H} = 0.50$ ML) is energetically favorable and, due to the small energy barrier within the reaction, will occur at a fast rate.

In similar circumstances to the previously described clean surface, the adsorption of molecular hydrogen on a $\theta_S = 0.25$ ML surface (Figure 7) is exothermic in nature but not quite as stable. On a $\theta_S = 0.25$ ML surface, the combined kinetic barriers necessary to produce $\theta_{2H} = 0.25$ ML require 4 kcal/mol of energy, but release only 9 kcal/mol of thermodynamic energy. When comparing molecular hydrogen adsorption on the two surfaces, $\theta_S = 0$ ML and $\theta_S = 0.25$ ML, the energy released during the respective reaction on the $\theta_S = 0$ ML surface is considerably larger and therefore more likely to occur. A maximum hydrogen surface coverage of only $\theta_{2H} = 0.25$ ML is reached due to the large steric interactions between the adsorbed hydrogens and the adsorbed sulfur atom on the surface.

The adsorption of molecular hydrogen on a $\theta_S = 0.50$ ML surface (Figure 7) produces a completely different picture to the sulfur coverages previously described ($\theta_S = 0$ and 0.25 ML). While also being an endothermic reaction (+14 kcal/mol) the combined energy barriers necessary to produce even a $\theta_{2H} = 0.25$ ML surface are sufficiently large (16 + 30 = 46 kcal/mol) to bring into question the feasibility of the reaction.

3.4.1. Comparing the Thermodynamic and Kinetic Pathway Produced during Molecular Hydrogen Adsorption at Different Sulfur Surface Coverages. After determining the maximum adsorption of molecular hydrogen at increasing sulfur surface coverage, we now consider the individual steps in the reaction mechanism on each corresponding *n**S surface ($n = 0, 1, 2$).

Geometries and energy profiles concerning structures involved in molecular hydrogen adsorption ($n = 0$) are presented in Figure 6a−f, Figure 7 ($\theta_{2H} = 0-0.25$ ML), and Figure 8 ($\theta_{2H} = 0.25-0.50$ ML). Molecular hydrogen is initially adsorbed onto a clean surface using a 1f coordination site (TS, Figure 6a; energy barrier, +1.4 kcal/mol). Hydrogens within the resulting minima structure, Figure 6b, are positioned 1.52 Å from the nickel surface atom. The bond between the hydrogen atoms is broken, and the H−H distance is elongated from 0.75 to 0.92 Å, comparing the $H_2(g)$ and *H*H′ species, respectively. It should be noted that unlike corresponding reaction pathways on the $\theta_S = 0.25$ ML and $\theta_S = 0.50$ ML surfaces (described further on in the account), this surface does not involve the formation of "HH_3f" species. Subsequent steps involve migration of the hydrogen atoms to 3f positions; first to adjacent 3fh sites (Figure 6d, *H−*H) and then to opposing 3fh and 3ff positions (Figure 6f, *H--*H). Both structures retain Ni−H bonds of ~1.70 Å. The second molecule of hydrogen to adsorb on the surface also adsorbs using a 1f geometry (TS, Figure 8a; energy barrier, +3.5 kcal/mol). For further adsorption of molecular hydrogen to occur, the existing hydrogens adsorbed on the surface must first rearrange to the previously described "H_H" configuration. This accounts for the least amount of surface steric interactions between the adsorbed hydrogens once adsorption occurs (Figure 8b, *H-*H-*H*H). Upon formation, this *H-*H-*H*H species readily undergoes one further reaction to produce a more stable surface orientation (Figure 8c, 4*H(*H-*H-*H-*H)). This symmetrical species, containing hydrogen atoms in all 3fh sites, produces Ni−H bonds of 1.67 Å. Despite remaining a considerably exothermic reaction, the energy barriers to hydrogen adsorption increase with the number of adsorbed hydrogen atoms.

Molecular hydrogen adsorption on the $\theta_S = 0.25$ ML surface ($n = 1$) is described in Figure 6g−l based on the corresponding geometries and in Figure 7 using the thermodynamic and kinetic pathway. In a manner very similar to the $\theta_S = 0$ ML surface, molecular hydrogen adsorbs in a 1f position (TS, Figure 6g; energy barrier, +1.7 kcal/mol). The corresponding bond distances in the resulting *S−*H*H′ structure (Figure 6h) are as follows: Ni−H (×2) 1.65 Å and Ni−S (×2) 2.15 and 2.18 Å. On the basis of the Ni−H bond distances and in contrast to the corresponding 1f structure on the $\theta_S = 0$ ML surface (also demonstrated by adsorption energies described in Section 3.3, Table 1), hydrogen atoms are not adsorbed to the surface as strongly in the presence of sulfur. Migration of the hydrogen atoms to adjacent 3f sites (TS, Figure 6i) leads to a "HH_3f" structure not seen on the previous $\theta_S = 0$ ML surface. This *S−*H*H structure (Figure 6j) retains very similar Ni−S bond distances of between 2.12 and 2.17 Å. The corresponding Ni−H bond distances are 1.60/1.61 and 1.72/1.68 Å, for H_{3fh}/H_{3ff} atoms, respectively. One last reaction step (TS, Figure 6k) produces the most stable unit cell structure containing one sulfur atom and two hydrogen atoms adsorbed on the surface, *S−*H−*H (Figure 6l). The "S_H_H" structure has been previously described in Section 3.3.

The geometries of molecular hydrogen adsorption on a $\theta_S = 0.50$ ML surface ($n = 2$) are illustrated in Figure 6m−p, while the corresponding reaction energies are described in Figure 7. Under identical circumstances to the previously described surfaces, molecular hydrogen adsorbs using 1f coordination to the surface (TS, Figure 6m; energy barrier, +30.2 kcal/mol). The resulting *S−*S−*H*H′ structure (Figure 6n) has a slightly

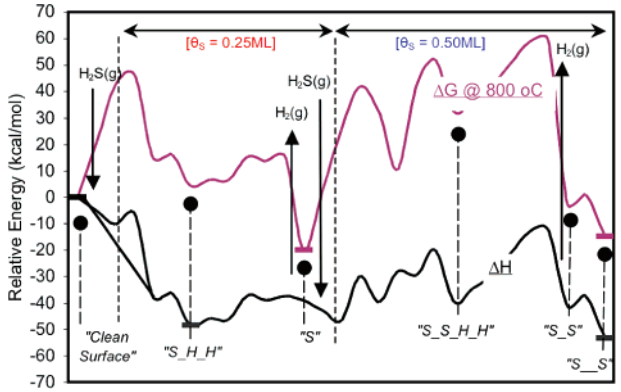

Figure 9. Overall energy pathway following consecutive adsorption of $H_2S(g)$ followed by desorption of $H_2(g)$, based on eqs 7−10. Energy profiles illustrated without entropy contributions (enthalpy, ΔH) and including entropy contributions at 800 °C (Gibbs' free energy, ΔG).

different geometry and is very endothermic in nature when compared to "HH_1f" structures of other *n**S surfaces. Unlike the corresponding structures in previous surfaces, the Ni−H bond distances in *S−*S−*H*H′ are not identical at 1.56 and 1.63 Å and the respective Ni−S bond distances are elongated to between 2.17 and 2.51 Å. One main reason for this difference in geometry and energy is due to the substantial sulfur−sulfur interaction on the surface, resulting in a S−S bond distance of 2.11 Å. The ensuing reactions on this surface first produce *S−*S−*H*H (Figure 6o) and then *S−*S−*H−*H (Figure 6p) minima structures. The *S−*S−*H*H structure maintains elongated Ni−S bonds of between 2.22 and 2.57 Å, while the S−S bond distance has increased to 2.17 Å. Compared to *S−*S−*H*H′ previously described, *S−*S−*H*H has substantially shorter and longer Ni−H bonds of between 1.54 and 1.90 Å. Minima structures, by definition, require a transition state as a prerequisite to formation. Despite this, after formation of S−S−*H*H′, no transition states could be determined during the calculation of respective mechanisms forming the *S−*S−*H*H and *S−*S−*H−*H species. The "S_S_H_H" structure has been previously described in Section 3.3.

3.5. Consecutive Hydrogen Sulfide and Molecular Hydrogen Adsorption on Nickel Surface.

$$\text{Surface} + H_2S(g) \leftrightarrow *SH_2 \leftrightarrow *SH-*H \leftrightarrow *S-*H-*H \quad (7)$$

$$*S-*H-*H \leftrightarrow *S-*H*H(') \leftrightarrow *S + H_2(g) \quad (8)$$

$$*S + H_2S(g) \leftrightarrow *S-*SH_2 \leftrightarrow *S-*SH-*H(') \leftrightarrow *S-*S-*H-*H \quad (9)$$

$$*S-*S-*H-*H \leftrightarrow *S-*S-*H*H(') \leftrightarrow *S-*S + H_2(g) \leftrightarrow *S--*S + H_2(g) \quad (10)$$

$$\text{Surface} + H_2(g) \leftrightarrow *H*H' \leftrightarrow *H-*H \leftrightarrow *H--*H \quad (11)$$

$$*H--*H + H_2(g) \leftrightarrow *H-*H-*H*H' \leftrightarrow *H-*H-*H-*H \quad (12)$$

On the basis of research previously described in this paper, we are able to produce an energy profile (Figure 9, eqs 7−10) illustrating optimum surface coverage produced by means of consecutive hydrogen sulfide adsorption followed by molecular hydrogen desorption on a planar nickel (111) surface. The corresponding reaction pathway takes into account the following reactions (eqs 7−10). Adsorption and dissociation of hydrogen sulfide (eq 7) on a clean surface generates species "S_H_H" (a combined surface of $\theta_S = 0.25$ ML/$\theta_{2H} = 0.25$ ML). Desorption of molecular hydrogen, from "S_H_H", maintains a surface of $\theta_S = 0.25$ ML by producing species "S" (eq 8). To produce a 0.50 ML coverage of sulfur, "S" can be used as a starting surface for further adsorption and dissociation of hydrogen sulfide, constructing species "S_S_H_H" and a combined surface of $\theta_S = 0.50$ ML/$\theta_{2H} = 0.25$ ML (eq 9). The desorption of molecular hydrogen from "S_S_H_H" maintains the $\theta_S = 0.50$ ML surface, initially producing structure "S_S". In turn, this species undergoes surface rearrangement to produce "S−−S" (eq 10). Adsorption of multiple molecules of molecular hydrogen (eqs 11−12) will also occur on the clean surface (reaction pathway illustrated in Figure 7 and Figure 8), up to a hydrogen surface coverage of $\theta_{2H} = 0.50$ ML.

This profile (Figure 9) highlights several key points concerning sulfur adsorption reactions occurring at the SOFC anode. The first key point (A) concerns maximum surface sulfur coverage on planar nickel. Despite substantial transition state barriers occurring during subsequent reaction steps, it is the exothermic nature of the overall reaction that is the driving force to produce a predominantly "S−−S" surface coverage (2*S equals a $\theta_S = 0.50$ ML surface). This is in agreement with experimental literature that determined the surface coverage of sulfur to be between 50−60%.[4,5,7−11a,16a] The second key point (B) involves the reversibility of the hydrogen sulfide adsorption reaction. Once maximum sulfur surface coverage has been reached, desorption of hydrogen sulfide is achieved experimentally by removing $H_2S(g)$ from the anode fuel feed.[7,16a,19,20] However, some research groups have demonstrated only a partial removal of adsorbed sulfur from the surface in this manner.[16a,19,20] There are two energy profiles illustrated in Figure 9. One is constructed from enthalpy data (ΔH, black line), which is not temperature dependent. The other is constructed from temperature-dependent Gibbs' free energy data ($\Delta G = \Delta H - T\Delta S$, purple line) and is based on a standard SOFC operating temperature of 800 °C. The $T\Delta S$ contribution for the gas molecules $H_2S(g)$ and $H_2(g)$ is $T\Delta S_{H2S(g)} = 52.7$ kcal/mol and $T\Delta S_{H2(g)} = 33.5$ kcal/mol, respectively. For all other species in the reaction pathway, the $T\Delta S$ contribution is set to zero. On the reaction pathway constructed from enthalpy data, "S_H_H" is the most stable intermediate species on the $\theta_S = 0.25$ ML surface. On the corresponding $\theta_S = 0.50$ ML surface the most stable species is "S−−S". Taking into account entropy contributions, an identical reaction pathway constructed from Gibbs' free energy determines that the most stable surface intermediate species are "S" and "S−−S" on the $\theta_S = 0.25$ and 0.50 ML surface, respectively. On the basis of the pathway described in Figure 9, the difference in relative energy between the most stable species at each coverage of adsorbed sulfur (0.25 and 0.50 ML) is very small; the enthalpy/entropy difference is −5/+5 kcal/mol, respectively. This almost negligible difference between the two surfaces, coupled with the large initial surface concentration of "S−−S", causes the readsorption of molecular hydrogen and desorption of one molecule of hydrogen sulfide per surface unit cell ($\theta_S = 0.50-0.25$ ML) to occur with relative ease. This data illustrates the partial reversibility of the hydrogen sulfide adsorption reaction, from 50 to 25% sulfur surface coverage. The relative energy difference between the clean surface and the most stable species on the $\theta_S = 0.25$ ML surface is considerably larger; the enthalpy/entropy difference is +48/+20 kcal/mol, respectively. For the complete removal of surface sulfur to occur via desorption of hydrogen sulfide, a substantial amount of energy would have to be introduced into the system to accomplish this exceptionally large endothermic reaction. Even taking into account the energy introduced into the SOFC

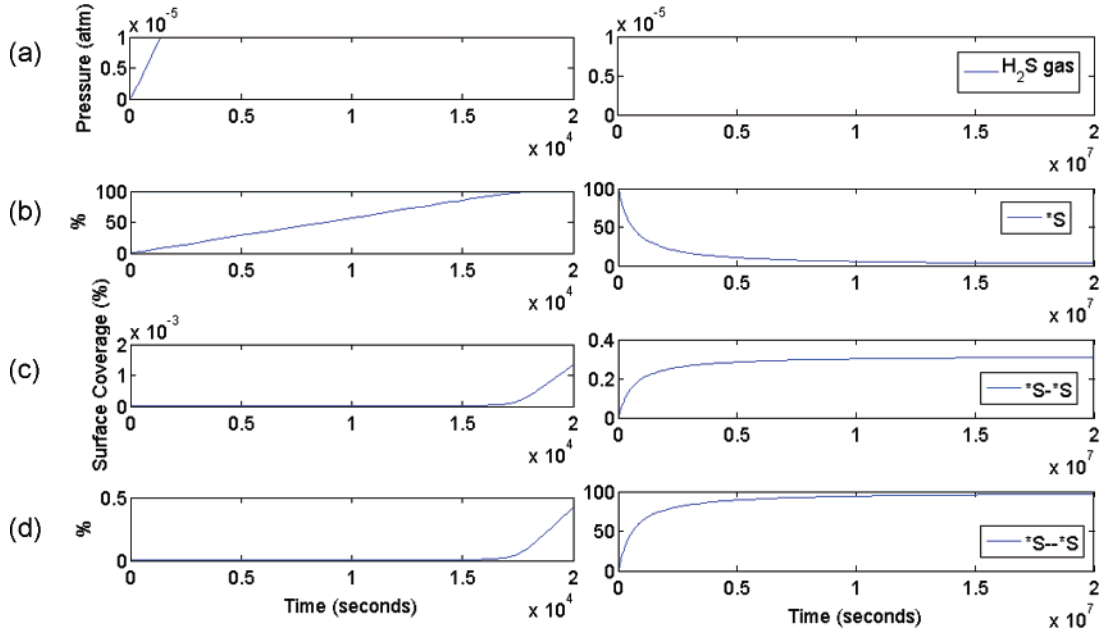

Figure 10. Graphical representation of individual surface coverage of selected species determined by kinetic model A, based on eqs 7−12. Left and right graphs illustrate different time periods, 2×10^4 and 2×10^7 seconds, respectively.

due to temperature (entropy), the removal of the remaining 25% sulfur surface coverage could not occur using this model.

To prove the validity of these two key points, we use a kinetic approach to describe the adsorption/desorption reactions occurring at the SOFC anode. This method describes each reaction step and its corresponding kinetic barrier (eqs 7−12) as mathematical equations, based on the Eyring equation and using the mathematical software MatLab[32] (see Section 2.2.). The equations represent a SOFC by means of a continually stirred tank reactor (CSTR) model. Our CSTR model can be considered as a "box" (mimicking the anode) with a volume of 1.35×10^{-6} m^3, maintained at a temperature of 800 °C (typical SOFC operating temperature). The reactive surface within the CSTR (mimicking the anode surface) has a 6.75×10^{-1} m^2 surface area and a vacant adsorption site concentration of 7.72×10^{-6} mol/m^2 (based on the number of 3f sites on a nickel (111) surface). Gaseous fuel (anode fuel feed) continually flows into the CSTR and gaseous products or unused fuel (anode byproducts) continually flow out with a flowrate of 40 mL/min STP. Inside the CSTR, gaseous species can adsorb and be desorbed from the surface, and adsorbed species can react with each other (anode reactions described in eqs 7−12). The CSTR reactive surface is hypothetically dissected into small equally sized sections, corresponding to four nickel atoms and their surrounding space. Four nickel atoms per section were chosen to mimic the size of the nickel unit cell (2×2) used during calculations. Each of these 'sections" represents one vacant site on the CSTR surface. By means of this method, we can consider steric interactions between adsorbed species on the CSTR surface. Adsorbing and dissociating species within one vacant site maintains the correct surface coverage within that adsorption site. For example, a 100% CSTR surface coverage of a 2*S species ($\theta_S = 0.50$ ML surface) produces an overall surface with 50% sulfur coverage. Through the use of this CSTR model, the ever changing concentrations of all gaseous and adsorbed species pertaining to adsorption/desorption reactions on the SOFC anode can be calculated until surface coverage equilibrium is reached.

The first kinetic profile (A) we considered describes reactions illustrated in eqs 7−12 with an anode fuel feed comprised of ~1atm H_2(g) and 10 ppm H_2S(g). Kinetic profile A models the key point A described above. This accounts for all reactions concerning the adsorption/desorption of hydrogen sulfide and the subsequent adsorption/desorption of molecular hydrogen on a planar nickel surface up to a sulfur surface coverage of 50%. All initial concentrations of the adsorbed species are set to zero. The most important data from this kinetic profile demonstrates that hydrogen sulfide adsorption and subsequent molecular hydrogen desorption initially produce a 25% sulfur surface coverage (Figure 10b, 100% CSTR surface coverage of $\theta_S = 0.25$ ML surface species "S"). Further molecules of hydrogen sulfide are adsorbed on the surface, creating a 50% sulfur surface coverage only once "S" reaches a CSTR coverage of 100%. Surface equilibrium is reached upon the production of a 50% sulfur surface coverage (Figure 10d, 100% CSTR surface coverage of $\theta_S = 0.50$ ML surface species "S−−S") with no remaining hydrogen adsorbed on the surface. This kinetic model proves the validity of the first key point described above: that an overall surface coverage of 50% could be attained on a nickel (111) surface. Both Sasaki[19] and Birss[20] have experimentally demonstrated that there are two stages of sulfur poisoning on nickel surfaces, regardless of temperature or hydrogen sulfide concentration. The first stage encompasses an initial, abrupt reduction in activity. The second stage comprises of a larger, gradual decrease in activity. We believe that this phenomenon can also be explained by the data in kinetic model A. The first stage accounts for the rapid production of a sulfur surface coverage of 25% (Figure 10b). The abrupt drop in cell activity is due to the considerably exothermic nature of hydrogen sulfide adsorption, and the reduction in molecular hydrogen adsorption that can favorably occur once the $\theta_S = 0.25$ ML surface has been achieved (see Section 3.3). Further, slower, adsorption of hydrogen sulfide, to eventually produce a maximum $\theta_S = 0.50$ ML surface, depicts the second stage in surface sulfur poisoning (Figure 10d). The explanation for the slow decrease in activity during the second stage is due to higher kinetic barriers associated with hydrogen sulfide adsorption on a sulfur surface coverage of 25%.

The second kinetic profile (B) we considered describes reactions illustrated in Figure 9 with an anode fuel feed

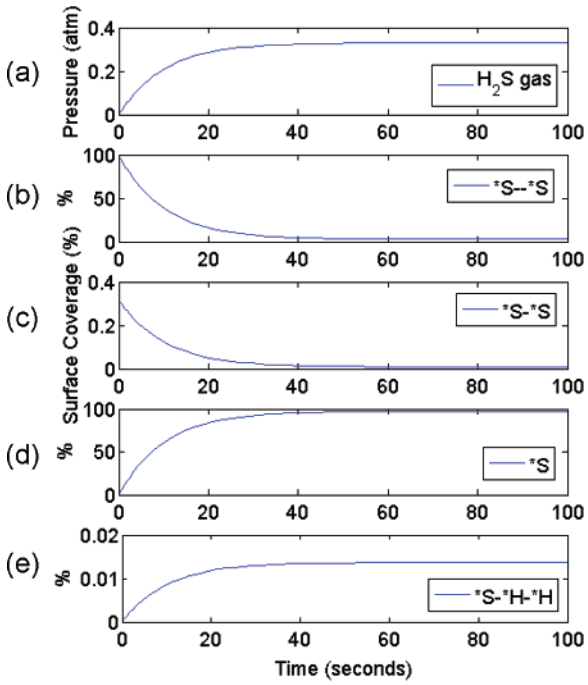

Figure 11. Graphical representation of individual surface coverage of selected species determined by kinetic model B, based on eqs 7−12.

comprised of 1atm H_2(g) and an initial 100% CSTR surface coverage of the species "S−−S". Kinetic profile B models the key point B described above. This model mimics experimental attempts to purge sulfur from the surface by eliminating H_2S-(g) from the anode feed once a maximum sulfur surface coverage of 50% has been attained. All initial concentrations of adsorbed species are set to zero, except "S−−S". The most important results for this model (Figure 11) illustrate the partial irreversibility of hydrogen sulfide adsorption on a nickel (111) surface. The initial 100% CSTR surface coverage of $\theta_S = 0.50$ ML surface species "S−−S" is reduced to zero (Figure 11b), as hydrogen adsorbs on the surface (eq 10) and hydrogen sulfide desorbs from the surface (eq 9). Upon the production of a 100% CSTR surface coverage of the $\theta_S = 0.25$ ML surface species "S", equilibrium is reached. The endothermic nature of subsequent hydrogen sulfide desorption reactions disallows the removal of all the adsorbed surface sulfur.

4. Conclusions

Sulfur-based contaminants (e.g., hydrogen sulfide) within the anode fuel feed substantially decrease the overall electrochemical performance of the SOFC.[1,6,7,16a,19,20] Reduction in cell activity is due to anode degradation caused by small amounts (parts per million) of sulfur compounds adsorbing on the anode surface. Despite the adsorption of these strongly bound sulfur atoms, SOFC activity is reduced but not eliminated. The failure of sulfur to cause completely inoperable conditions within the SOFC anode is due to the inability of planar nickel to favorably adsorb hydrogen sulfide at a sulfur surface coverage greater than 50% (Ni/S_{ads} surface ratio, 2:1). This inability can be explained by thermodynamic data illustrating the endothermic nature of hydrogen sulfide adsorption reactions after 50% sulfur surface coverage is obtained. Our findings are in agreement with experimental research that has determined a maximum sulfur surface coverage of between 50 and 60% during reactions concerning the adsorption of hydrogen sulfide on a nickel surface.[4,5,7−11a,16a] The question of irreversible hydrogen sulfide adsorption on a nickel surface is important when pertaining to the removal of surface sulfur. Experimental studies have concluded that sulfur removal can occur by the temporary exclusion of contaminants from the anode feed.[7,16a,19,20] Desorption of hydrogen sulfide, from the predominantly sulfur-covered anode surface, occurs when the anode fuel is comprised of only hydrogen. Whether adsorption of hydrogen sulfide is a completely irreversible reaction has been considered by several research groups due to their inability to regain original electrochemical activity by means of this method.[16a,19,20] We have demonstrated that complete irreversibility of the hydrogen sulfide adsorption reaction is due to the difference in relative thermodynamic stability between the most stable species from each sulfur surface coverage studied (0, 25, and 50%). With or without the inclusion of temperature-dependent entropy contributions to the reaction energy, there is a substantial difference in relative energy (>20 kcal/mol) between the most stable species representing 0 and 25% sulfur coverages. On the other hand, there is only ∼5 kcal/mol in thermodynamic energy separating sulfur surface coverages of 25 and 50%. If upon formation of a surface coverage of 50% sulfur H_2S(g) is removed from the predominantly hydrogen SOFC anode feed, partial hydrogen sulfide desorption will occur up to a sulfur surface coverage of only 25%. This is due to the large initial concentration of sulfur species on the surface, coupled with the small relative energy difference between the corresponding sulfur surface coverages (25 and 50%). When attempting to remove further amounts of sulfur from the surface, the large difference in relative energy between coverages of 0 and 25% surface sulfur makes this an impossible reaction. Another consideration is the general adsorption energies of the species, depending on the sulfur surface coverage. We have determined that the larger the number of sulfur atoms surrounding an adsorbed species, the weaker the surface adsorption. Another main topic of our research considers the influence of adsorbed surface sulfur on the effectiveness of molecular hydrogen adsorption. Because of surface hydrogen adsorption being the prerequisite to the oxidation of hydrogen at the anode TPB, the success of molecular hydrogen adsorption is directly related to the activity of the SOFC. We have concluded that without the presence of sulfur on the surface, a hydrogen surface coverage of 50% ($Ni/2H_{ads}$ surface ratio, 2:1) is achieved at equilibrium. Due to the very exothermic nature of molecular hydrogen adsorption at a sulfur surface coverage of 0%, equilibrium occurs without delay. At 25 and 50% sulfur surface coverages, adsorption of molecular hydrogen creates a hydrogen surface coverage of only 25% ($Ni/S_{ads}/2H_{ads}$ surface ratio, 4:1:1 and 4:2:1, respectively). While the presence of increasingly larger amounts of surface sulfur reduces the exothermic nature of hydrogen adsorption, kinetic barriers to adsorption increase. Despite experimental data showing a small but considerable decrease in cell activity due to sulfur-based contaminants in the SOFC anode fuel feed, we have demonstrated that molecular hydrogen adsorption on a nickel surface can be reduced by up to 50% due to the presence of adsorbed sulfur on the surface.

Acknowledgment. Financial support was provided by the Alberta Energy Research Institute and the Western Economic Diversification Department. All calculations were carried out on WestGrid computing resources, funded in part by the Canada Foundation for Innovation, Alberta Innovation and Science, BC Advanced Education, and the participating research institutions. The WestGrid equipment was provided by IBM, Hewlett-Packard, and SGI.

Supporting Information Available: Rate of formation derivations for individual species and calculated reaction rate constants within kinetic profiles A and B. Pictorial representation of relaxed sulfur/nickel "zigzag" surface layer. Thermodynamic energy profiles concerning multiple adsorptions of molecular hydrogen ($\theta_{2H} \sim 0-1$ ML) on n*S-Surface ($n = 0, 1, 2$). This material is available free of charge via the Internet at http://pubs.acs.org.

References and Notes

(1) (a) Steele, B. C. H.; Heinzel, A. *Nature* **2001**, *414*, 345. (b) Ormerod, R. M. *Chem. Soc. Rev.* **2003**, *32*, 17. (c) McIntosh, S.; Gorte, R. J. *Chem. Rev.* **2004**, *104*, 4845. (d) Atkinson, A.; Barnett, S.; Gorte, R. J.; Irvine, J. T. S.; McEnvoy, A. J.; Mogensen, M.; Singhal, S. C.; Vohs, J. *Nat. Mater.* **2004**, *3*, 17. (e) Johnston, B.; Mayo, M. C.; Khare, A. *Technovation* **2005**, *25*, 569.

(2) (a) Hirschenhofer, J. H.; Stauffer, D. B.; Engleman, R. R.; Klett, M. G. *Fuel Cell Handbook*, 7th ed.; http://www.fuelcells.org/info/fclib.html (March 2007); p 7-4. (b) Matsuzaki, Y.; Yasuda, I.; *SOFC VII*, Proceedings of the 7th International Symposium of the Electrochemical Society, Pennington, NJ, 2001, vol. 2001-16, p. 769.

(3) McCarrol, J. J.; Edmonds, T.; Pitkethly, R. C. *Nature* **1969**, *223*, 1260.

(4) Bordoli, R. S.; Vickerman, J. C.; Wolstenholme, J. *Surf. Sci.* **1979**, *85*, 244.

(5) Alstrup, I.; Rostrup-Nielsen, J. R.; Røen, S. *Appl. Catal.* **1981**, *1*, 303.

(6) Bartholomew, C. H.; Pannell, R. B. *Appl. Catal.* **1982**, *2*, 39.

(7) Fitzharris, W. D.; Katzer, J. R.; Manogue, W. H. *J. Catal.* **1982**, *76*, 369.

(8) Blaszczyszyn, M.; Blaszczyszyn, R.; Meclewski, R.; Melmed, A. J.; Madey, T. E. *Surf. Sci.* **1983**, *131*, 433.

(9) (a) Rostrup-Nielsen, J. R. *J. Catal.* **1984**, *85*, 31. (b) Rostrup-Nielsen, J. R. Catalytic Steam Reforming. *Catalysis, Science, and Technology*; Anderson, J. R., Boudart, M., Eds., Springer-Verlag: New York, 1984; p 130.

(10) McGrath, R.; MacDowell, A. A.; Hashizume, T.; Sette, F.; Citrin, P. H. *Phys. Rev. B.* **1989**, *40*, 9457.

(11) (a) Huntley, D. R. *Surf. Sci.*, **1990**, *240*, 13−23. (b) Huntley, D. R. *Surf. Sci.* **1990**, *240*, 24.

(12) Oed, W.; Starke, U.; Heinz, K.; Müller, K.; Pendry, J. B. *Surf. Sci.* **1991**, *488*, 251−252.

(13) Marécot, P.; Paraiso, E.; Dumas, J. M.; Barbier, J. *Appl. Catal., A* **1992**, *80*, 89.

(14) Gardin, D. E.; Batteas, J. D.; Van Hove, M. A.; Somorjai, G. A. *Surf. Sci.* **1993**, *296*, 25.

(15) Papageorgopoulos, C. A.; Kamaratos, M. *Surf. Sci*. **1995**, *338*, 77.

(16) (a) Hepola, J.; Simell, P. *Appl. Catal., B.* **1997**, *14*, 305. (b) Hepola, J.; McCarty, J.; Krishnan, G.; Wong, V. *Appl. Catal., B.* **1999**, *20*, 191.

(17) Maurice, V.; Kitakatsu, N.; Siegers, M.; Marcus, P. *Surf. Sci.* **1997**, *373*, 307.

(18) Capitano, A. T.; Cland, J. L *J. Phys. Chem. B* **1999**, *103*, 6573.

(19) Sasaki, K.; Susuki, K.; Iyoshi, A.; Uchimura, M.; Imamura, N.; Kusaba, H.; Teraoka, Y.; Fuchino, H.; Tsujimoto, K.; Uchida, Y.; Jingo, N. *J. Electrochem. Soc.* **2006**, *153*, A2023.

(20) Smith, T. R. Ph.D. Thesis, University of Calgary, Calgary, Alberta, Canada, 2007.

(21) Chesters, M. A.; Lennon, D.; Ackermann, L.; Häberlen, O.; Krüger, S.; Rösch, N. *Surf. Sci.* **1993**, *291*, 177.

(22) Yang, H.; Whitten, J. L. *Surf. Sci.* **1997**, *370*, 136.

(23) (a) Choi, Y. M.; Compson, C.; Lin, M. C.; Liu, M. *Chem. Phys. Lett.* **2006**, *421*, 179. (b) Choi, Y. M.; Compson, C.; Lin, M. C.; Liu, M. *J. Alloys Compd.* **2007**, *427*, 25.

(24) Marquez, A. I.; De Abreu, Y.; Botte, G. G. *Electrochem. Solid State Lett.* **2006**, *9*, A163.

(25) Albenze, E. J.; Shamsi, A. *Surf. Sci.* **2006**, *600*, 3202.

(26) (a) Kresse, G.; Hafner, J. *Phys. Rev. B: Solid State* **1993**, *48*, 13115. (b) Kresse, G.; Hafner, J. *Phys. Rev. B: Solid State* **1994**, *49*, 14251. (c) Kresse, G.; Furthmüller, J. *Comput. Mater. Sci.* **1996**, *6*, 15. (d) Kresse, G.; Furthmüller, J. *Phys. Rev. B: Solid State* **1996**, *54*, 11169.

(27) (a) Blöchl, P. E. *Phys. Rev. B: Solid State* **1994**, *50*, 17953. (b) Kress, G.; Joubert, D. *Phys. Rev. B: Solid State* **1999**, *59*, 1758.

(28) Perdew, J. P.; Burke, K.; Ernzerhof, M. *Phys. Rev. Lett.* **1996**, *77*, 3865.

(29) Monkhorst, H. J.; Pack, J. D. *Phys. Rev. B: Solid State* **1976**, *13*, 5188.

(30) Villars, P.; Calvert, L. D. *Pearson's Handbook of Crystallographic Data for Intermetallic Phases*; American Society of Metals: Metals Park, OH, 1985.

(31) Jónsson, H.; Mills, G.; Jacobsen, K. W. Nudged elastic band method for finding minimum energy paths of transitions. In *Classical and Quantum Dynamics in Condensed Matter Phase Simulations*; Berne, B. J., Ciccotti, G., Coker, D. F., Eds.; World Scientific: Singapore, 1998; p 385.

(32) *MatLab* software (version 6.5.1. release 13, Service Pack 1) situated on the "Lattice" group of computers, part of the Westgrid facility. www.mathworks.com (accessed March 2007).

(33) (a) Baerends, E. J. Ph.D. Thesis, Free University, Amsterdam, The Netherlands, 1973. (b) Baerends, E. J.; Ellis, D. E.; Ros, P. *Chem. Phys.* **1973**, *2*, 41.

(34) (a) Becke, A. *Phys. Rev. A: At., Mol., Opt., Phys.* **1988**, *38*, 3098. (b) Perdew, J. P. *Phys. Rev. B: Condens. Mater.* **1986**, *34*, 7406. (c) Perdew, J. P. *Phys. Rev. B: Condens. Mater.* **1986**, *33*, 8822.

(35) Sun, M.; Nelson, A. E.; Adjaye, J. *Catal. Lett.* **2006**, *109*, 133.